Cul5^{Wsb2} uses BCL2 proteins as co-receptors to target Bim for degradation.

Wilhelm Vaysse-Zinkhöfer[**1], Enya Marie Catherine Alcindor[1], Nicholas Garaffo[2] and David Paul Toczyski*[1,3]**
Helen Diller Family Cancer Center
University of California, San Francisco
1450 3rd Street
San Francisco, CA 94158

[1]Department of Biochemistry, Helen Diller Family Comprehensive Cancer Center, University of California, San Francisco, CA, USA
[2]Massachusetts General Hospital Cancer Center, Harvard Medical School (HMS), Boston, MA, USA
[3]Lead contact

*Correspondence: dpt4darwin@gmail.com
**Correspondence: Wilhelm.vaysse-zinkhofer@ucsf.edu

SUMMARY

Apoptosis helps eliminate damaged or unnecessary cells. Anti-apoptotic BCL2 family proteins protect cells by binding and inhibiting pro-apoptotic proteins. Our study reveals that BCL2 proteins also target Bim for degradation by serving to recruit Bim to the E3 ubiquitin ligase $Cul5^{Wsb2}$. Wsb2 recognizes Bcl-xl through a motif conserved between Bcl-xl, Bcl-w and Bcl2, but not Mcl1. Disruption of this interaction through mutation of either Bcl-xl or Wsb2 blocks the binding of Wsb2 to the Bcl-xl/Bim dimer. Wsb2 also associates with the Mcl1/Bim dimer through a separate Wsb2 interface, suggesting that Wsb2 has evolved independent means to target Bim. While Wsb2 is not essential in most cells, it is essential in cells derived from tumors of the nervous system, and knockdown of Wsb2 in these lines causes death by apoptosis. This work uncovers a novel mechanism of apoptosis regulation, with implications for developing therapies against neuroblastomas and other cancers reliant on this pathway for survival.

KEYWORDS

Wsb2, Ubiquitin, Apoptosis, Neuroblastoma, Cancer

Introduction

The apoptosis pathway triggers cell death in response to either extracellular or intracellular signals[1]. Apoptosis is mediated by Bax, Bok and Bak, which oligomerize to form pores in the outer mitochondrial membrane through their four BH domains[1–3]. Antagonizing this event are a set of anti-apoptotic proteins (Bcl2, Bcl-xl, Bcl-w, Mcl1, and Bfl-1/A1) which use these same domains to bind pore-forming proteins and block their oligomerization[1,4]. This event is further regulated by two sets of proteins that contain only one BH domain, BH3. One set of these "BH3-only" proteins (e.g. Bid, Bim and Puma), also known as “activators”, binds and activates the pore formers directly, and also binds and interferes with anti-apoptotic BCL2-like proteins[5–9]. The second set of BH3-only proteins (e.g. Noxa, Bad and Bik) sequester the anti-apoptotic BCL2-like proteins, and thus activate apoptosis by inhibiting its inhibitors[1,5,9,10].
This fine balance of pro and anti-apoptotic factors is further regulated in myriad ways. Bim, a pro-apoptotic factor mutated in non-small cell lung cancer (NSCLC)[11–13], Leukemia[14,15] and Neuroblastomas[16], is regulated at the level of splicing, phosphorylation, localization and protein turnover[17]. Bim exists in three main splicing isoforms: extra-long (Bim_{EL}), long (Bim_L) and short (Bim_S)[17,18]. Amino acids encoded in exons specific to Bim_{EL} are phosphorylated by both Erk1/2 and Rsk1/2[19] (Fig. 2A). These phosphorylations promote the targeting of Bim_{EL} by the F box protein ßtrcp, which acts as a substrate specificity factor for the SCF[19]. The SCF is one of seven Cullin Ring Ligases (CRLs), each of which contains a different Cullin (Cul1 for the SCF) and one of two RING subunits (Rbx1 or Rbx2)[20–22]. The human genome encodes several hundred genes with domain structures that correspond to CRL substrate receptors, most of which are thought to be genuine CRL subunits[23]. Cul5 employs Rbx2, and two adaptors, EloB and EloC, which tether any of about 40 SOCS box to Cul5[24–26]. Each of the CRL ligases works in concert with a separate ubiquitin ligase that adds the first ubiquitin to the substrate. Most CRLs use Arih1 for this function, whereas the Cul5 ligase uses a paralog, Arih2[27–29]. Ubiquitin ligases are essential in a number of pathways involved in development, cell division, specification or migration[30] and are often mutated or amplified in tumors[31–34]. Consequently, significant efforts have been made to more readily identify their targets[35–38].
Anti-apoptotic BCL2 family members such as Bcl2, Bcl-xl, and Bcl-w have long been known to suppress apoptosis by binding, and thereby inhibiting, the function of pro-apoptotic BH3-only proteins[1,7,39,40]. We have found that Bcl-xl inhibits at least one pro-apoptotic BH3-only protein, Bim, by facilitating its degradation. Here, we show that the Cul5 substrate adaptor Wsb2 binds Bcl-xl directly and, through that interaction, targets the associated Bim for degradation without affecting the half-life of Bcl-xl itself. While Wsb2 is not essential in most primary or tumor cells, high-throughput DepMap data suggest it is critical for survival in tumors of the peripheral nervous system, such as neuroblastoma. We show loss of Wsb2 in neuroblastoma cells leads to a sudden and dramatic increase in apoptosis, suggesting that Wsb2 is a strong candidate for drug discovery in this class of cancers.

Results

Wsb2 and Cul5 mutants have high levels of Bim_{EL}, Bim_L and Bim_S splicing isoforms.

Previously, high throughput studies showed that mutation of Cul5, Rbx2, Arih2, or Wsb2 sensitized HAP1 cells to the mitochondrial complex II inhibitor TTFA[41], and Wsb2-depleted HAP1 cells displayed a growth defect after TTFA treatment (Fig. 1A). Additionally, analysis of dependency data from the DepMap consortium revealed that Wsb2 positively correlated with anti-apoptotic Bcl-w, Bcl2, Mcl1, Bcl-xl (Pearson’s corr > 0,2) and negatively correlated with pro-apoptotic PMAIP (Noxa) and Bax (Pearson’s corr < 0,2) (Fig. 1B), consistent with data from several CRISPR screens[42,43]. GO analysis of the top 100 Wsb2 co-dependencies revealed significant enrichment in apoptosis regulation (Fig. 1B). As these results suggested a potential role for Wsb2 in negative apoptosis regulation, we investigated the potential involvement of Wsb2 in this pathway.

Interactions between members of the BCL2 family are thought to dictate the inhibition or initiation of apoptosis. The BH3-only sensitizers/activators (Puma, Bik, Bad, Hrk, Bmf and Noxa) are upregulated through p53 and Myc in response to apoptotic stimuli such as DNA damage or mitochondrial stress[44,45]. These proteins subsequently bind the anti-apoptotic BCL2 proteins (Bcl2, Bcl-w, Bcl-xl, and Mcl1) freeing the BH3-only activators Bim and Bid and the effectors Bax and Bak, which are usually sequestered by the anti-apoptotic members. The release of Bim and Bid leads to the mitochondria outer membrane permeabilization (MOMP) through the activation of Bax and Bak, committing cells to apoptosis[3,4] (Fig. 1C).

To test Wsb2's function in this process, we generated clonal RPE1 cell lines with Wsb2 or Cul5 mutations, confirmed by sequencing (Fig. S1A) and, for Cul5, by immunoblotting (Fig. 1D). Commercially available antibodies directed against Wsb2 were not functional, making direct detection challenging. To assess the impact of Wsb2 or Cul5 mutation on apoptotic protein levels, we probed immunoblots for a large panel of apoptotic proteins (Puma, Noxa, Bik, Bad, Bcl2, Bcl-w, Bcl-xl, Mcl1, Bid, Bim, Bak and Bax) as well as p53, March5, Cul5 and Cyclin-D1 (Fig. 1D). Immunoblotting analysis revealed a significant upregulation of all Bim isoforms and Puma signal, and a modest increase in the levels of Bcl2 in some experiments, across multiple independently derived Wsb2 and Cul5 mutants. In contrast, the steady state levels of Noxa, Bik, Bad, Bcl-w, Bcl-xl, Mcl1, Bid, Bak and Bax remained unchanged in the Wsb2 and Cul5 mutants. Moreover, the levels of March5 (a ubiquitin ligase important for apoptosis, whose mutation also rendered cells sensitive to TTFA[41]) and p53 were also unaffected. Although Ccnd1 has been suggested to be a potential substrate of Wsb2[46], no changes in Ccnd1 levels were observed. Treatment with 1uM Rotenone (mitochondrial complex I inhibitor) or 25nM Camptothecin (CPT; Topoisomerase I inhibitor) during a 48h time course leads to increased levels of cleaved Parp (c-Parp) in Wsb2 mutants compared to WT, while CPT treatment showed no effect (Fig. S1B), suggesting that Wsb2 mutant cells are sensitized to apoptosis induced by mitochondrial poisons. qPCR analysis showed reduced Wsb2 and Cul5 transcripts, consistent with nonsense-mediated decay[47] (Fig. 1E). However, Bim mRNA levels were unchanged, suggesting post-transcriptional regulation. Puma and Bcl2 mRNA were too low to quantify.

We then examined whether Bim or Puma were direct targets of Wsb2. We generated RPE1 cells expressing either untagged or 5xHA-tagged Wsb2 alleles under the control of a doxycycline-inducible promoter and induced expression for 8 hours. Immunoprecipitation with anti-HA antibody showed a robust co-immunoprecipitation with endogenous Bcl-xl and Bim_{EL}, and, more weakly, Mcl1. Bim_L and Bim_S were not detected, likely due to their low abundance in RPE1 cells (Fig. 1F). Despite evidence of Wsb2 regulating Noxa[48,49], Wsb2 depletion did not induce a change in Noxa steady state level and Noxa did not co-immunoprecipitate with Wsb2 .

Wsb2 regulates Bim through Bcl-xl and Mcl1

Bim_{EL} is a well-described target of the $SCF^{ß\text{-}TrCP1}$ complex, which recognizes and ubiquitinates Bim_{EL} after phosphorylation by Rsk1/2 and Erk1/2 (Fig. 2A). Meanwhile, Bim_L and Bim_S both lack the phosphorylation sites targeted by Rsk1/2 and Erk1/2, preventing them from being recognized and ubiquitinated by $SCF^{ß\text{-}TrCP1}$ [17,19] (Fig. 2A). To determine if Wsb2 is specifically interacting with the Bim_{EL} isoform, we introduced a doxycycline-inducible 3xFlag-tagged $Bim_{EL,}$ Bim_L or Bim_S constructs into RPE1 cells co-expressing either the 5xHA tagged or untagged Wsb2. Following a 3-hour Dox treatment, immunoprecipitation with anti-HA antibodies revealed that Wsb2 interacts with all Bim isoforms, albeit more weakly with Bim_S (Fig. 2B).

Strikingly, both Bcl-xl and Mcl1 showed increased interaction with Wsb2 upon Bim_{EL} overexpression (Fig. 2C), suggesting Wsb2 may specifically recognize a heterodimer, whereas Bcl-w and Bcl2 were expressed at too low a level to evaluate (Fig. S2A). The hydrophobic C-terminal E5 domain of Bim is conserved across all three isoforms (Fig. 2A) and is necessary for Bim's interaction with the mitochondria outer membrane[50]. We examined whether interaction with the mitochondria was required for Bim's interaction with Wsb2. A 3xFlag tagged truncated Bim_{EL} lacking the E5 domain (Bim E2A-E4) was overexpressed with or without 5xHA-Wsb2 . While the Bim E2A-E4 allele was very poorly expressed, it still bound to Wsb2, suggesting that this is independent of its interaction with the mitochondrial membrane (Fig. 2D, lanes 7/8 vs lanes 9/10). To determine whether Wsb2 interacts with Bcl-xl and Bim independently, or only within the context of the Bcl-xl/Bim heterodimer, we conducted a co-immunoprecipitation experiment in the absence of dimerization by pre-treating cells with the pan-BCL2 BH3-mimetic ABT-263 (Navitoclax) for 3 hours. BH3-mimetics selectively bind to the BH3 domain of anti-apoptotic BCL2-proteins, disrupting their interactions with pro-apoptotic BH3-only proteins, triggering apoptosis. ABT-263 selectively targets Bcl-xl, Bcl2 and Bcl-w. Disruption of the Bcl-xl/Bim complex led to a loss of the interaction of Wsb2 with Bcl-xl and Bim, suggesting that Wsb2's interaction with Bim is largely dependent on Bcl-xl (Fig. 2E).

To investigate the specificity of these interactions, cells were treated with the BH3 mimetics A1331852, S63845 and ABT199, which target Bcl-xl, Mcl1 and Bcl2, respectively. We carried out this experiment examining Bim_L due to its robust binding to Wsb2, and to eliminate any complication arising from $Bim_{EL,}$ which is targeted by both $Cul5^{Wsb2}$ and $SCF^{ßTRCP}$. Immunoprecipitation of FLAG-Bim_L confirmed that each inhibitor effectively disrupted the association between Bim and its respective target proteins (Fig. S2B). ABT-263 reduced Bcl-xl, Bcl-w, and Bcl2, but not Mcl1 in the FLAG-IP; A1331852 reduced only Bcl-xl; S63845 reduced Mcl1 (and Bcl2 very slightly); ABT199 reduced only Bcl2. Treatment with ABT-263 reduced the interaction between Wsb2 with both Bcl-xl and Bim_L, but

not with Mcl1. Treatment with S63845 disrupted the Wsb2-Mcl1 interaction, but not the Wsb2-Bcl-xl interaction. The A1331852 compound primarily disrupted the Wsb2-Bcl-xl interaction with a slightly less strong effect on Bim_L. This may be because, in the absence of Bcl-xl, Bim is redistributed to other BCL2 family members and is recognized by Wsb2 through these interactions. In contrast, ABT199 lead to a slight reduction of Wsb2-Bim_L interaction (Fig. 2F). Together, these results suggest that Wsb2 primarily targets Bim through the Bcl-xl/Bim and Mcl1/Bim complex, but can also recognize Bim in association with other apoptotic proteins.

Wsb2 regulates Bim independently of the ßTrCP1 pathway

To determine whether Wsb2 mutation affects apoptotic protein stability, we carried out a cycloheximide time course (Fig. 3A). Bim_{EL} and Bim_L were short-lived, whereas Bim_S was more stable. Bcl-xl, Bcl2, and Noxa (which undergoes a mobility shift) were stable. Loss of Wsb2 stabilized Bim but did not alter Bcl-xl or known Wsb2 substrates (Noxa, Ccnd1). Although Bim_S and Bcl2 levels were elevated in Wsb2 mutants (Fig. 1D), their half-lives were not markedly changed (Fig. 3A).

The longest form of Bim, $Bim_{EL,}$ is regulated through the MAPK pathway. Erk phosphorylates Bim_{EL} serines 59, 69 and 104, which then promotes Rsk-mediated phosphorylation of Bim_{EL} on the serines 93, 94 and 98[19]. This enables the recognition and subsequent ubiquitination of Bim_{EL} by the $SCF^{ßTRCP}$ complex. The more potent, smaller isoforms, Bim_L and $Bim_{S,}$ both lack the domains required for Rsk/Erk phosphorylation and regulation by $SCF^{ßTRCP1}$ (Fig. 2A). Given this, we were surprised to see Bim_{EL} entirely stabilized in the Wsb2 mutant. To determine if both $Cul5^{Wsb2}$ and $SCF^{ßTRCP}$ target Bim, we performed a time-course experiment following treatment with phorbol 12-myristate 13-acetate (PMA), which has been reported to drive Bim_{EL} destabilization through the Rsk/Erk/$SCF^{ßTRCP1}$ pathway[19]. As anticipated, treatment with PMA did not affect the stability of isoforms Bim_L and Bim_S. However, Bim_{EL} was destabilized in the Wsb2 mutant when PMA was added (Fig. 3B, Fig. S3A). Moreover, a noticeable phospho-shift was observed in Bim_{EL}, consistent with PMA activating Erk/Rsk mediated phosphorylation[19]. Interestingly, a phosphoshift of the stable Bim_L was also observed. To examine the turnover of monomeric Bim, we employed ABT-263. Addition of ABT-263 caused Bim degradation for all three isoforms, even in the Wsb2 mutant (Fig. 3C). This is unlikely to be due to $SCF^{ßTRCP}$ since this complex is only known to target the Bim_{EL} spliced form[19]. This suggests that yet another E3 targets monomeric Bim. Bim_{EL} (but not Bim_L or Bim_S) has been reported to be degraded by the proteasome even in the absence of poly-ubiquitination [51]. However, Wsb2-independent turnover in ABT-263 occurred for all three forms of Bim and was reduced by the neddylation inhibitor MLN4924, which inactivates CRL ligases, suggesting that targeting of the monomeric forms of Bim is requires, directly or indirectly, a CRL.

Although Wsb2 uses Bcl-xl to target Bim, Bcl-xl itself was stable. It may be that, under normal conditions, only a small fraction of Bcl-xl is bound to Bim and targeted by Wsb2. To test this hypothesis, we overexpressed Bim_{EL} for 3 hours before treating the cells with cycloheximide. Bim_{EL} overexpression led to only a modest destabilization of Bcl-xl in cycloheximide, suggesting that Bcl-xl is much less efficiently ubiquitinated (Fig. 3D). Consistent with previous observations (Fig. 2C), Bim_{EL} overexpression strongly increased and stabilized Mcl1[52,53].

To examine whether Bim is ubiquitinated by the $Cul5^{Wsb2}$ complex, we introduced a doxycycline-inducible Flag-Ubiquitin and a 13xMyc-Bim_L construct into RPE1 cells. We employed the Bim_L isoform because it lacked the confounding effects of being simultaneously targeted by $SCF^{ßTRCP1}$. Cells were treated with 100uM Z-VAD-FMK during the 8h induction with 1ug/ml doxycycline to prevent apoptosis. After harvesting, we performed an immunoprecipitation with anti-Myc antibodies and blotted for Flag-tagged (Ubiquitin) and Myc-tagged (Bim) proteins. Proteasome inhibitors were not used in these experiments, as we observed that their use led to the disruption of Wsb2 and Bim overexpression (Fig. S3B). Anti-Myc immunoprecipitation resulted in a high-molecular weight Flag-reactive smear indicative of polyubiquitination only when both Flag-ubiquitin and 13xMyc-Bim_L were co-expressed (Fig. 3E). Mutation of Wsb2 resulted in a reduction of the ubiquitin smear associated with Myc pull-down compared to wild type (Fig. 3E). These results suggest that $Cul5^{Wsb2}$ promotes Bim ubiquitination. Residual ubiquitination in the Wsb2 mutant may represent a high level of monomeric Bim seen upon overexpression.

Bim is targeted through a direct Wsb2-Bcl-xl interaction

Our results indicate that Wsb2 regulates Bim exclusively when in complex with another BCL2 family protein.

Based on our observation that Wsb2 regulates Bim via Bcl-xl, we used AlphaFold2 Multimer to predict potential Wsb2 interaction interfaces among monomeric BH3-containing apoptotic proteins. Alphafold[54] evaluates interface confidence (iPTM), domain positioning (PTM), and structural accuracy (PAE, pLDDT). We considered iPTM > 0.8; PTM > 0.5; PAE < 10 and pLDDT > 77 to be significant. As positive controls, EloB and EloC both showed high-confidence binding to Wsb2. Among 16 proteins tested, only Bcl-xl, Bcl2, and Bcl-w demonstrated strong interactions with Wsb2, whereas the Wsb2 paralog Wsb1 did not (Fig. 4A; Fig. S4A).
These predictions suggested that Wsb2 binds Bcl-xl via a DKEM motif (D156/K157/E158/M159) in Bcl-xl and an ERRRR motif (E28/R157/R174/R297/R353) in Wsb2 (Fig. 4B). The DKEM motif is conserved in Bcl2 and Bcl-w but is absent in Mcl1 and Bim_{EL} (Fig. 4C), and no direct Wsb2/Bim interaction was predicted (Fig. 4A). *In silico* alanine substitutions in the DKEM to K157A/E158A/M159A (Bcl-xl^{AAA}) or the ERRRR motif to R157E/R174E/R297E ($Wsb2^{EEE}$), abolished the predicted interaction (Fig. 4A, Fig. S4B). To validate these results, we generated doxycycline-inducible V5-tagged wild-type and these mutant alleles in a 3xFlag Bim_{EL} background. Despite the fact that the Bcl-xl^{AAA} allele expressed better than WT, it had reduced binding with Wsb2, but not Bim (Fig. 4D). Analogously, $Wsb2^{EEE}$ did not interact with Bcl-xl, but retained its interaction with Mcl1 (Fig. 4E; 4F). Our results suggest two distinct interaction mechanisms between Wsb2/Bcl-xl and Wsb2/Mcl1.

Wsb2 is essential in Neuroblastoma

While Wsb2 is expressed in various tissue types, its expression is highest in the nervous system, suggesting a potential role in safeguarding neuronal tissues from apoptosis (Fig. 5A). The Cancer genetic dependencies data from *The Cancer Map Dependency Project* (DepMap) show that tumors of the nervous system, Neuroblastomas and Malignant Peripheral Nerve Sheath Tumors (MPNSTs), are over-represented amongst those in which Wsb2 is essential for viability (Fig. 5B). There is a positive correlation (Pearson Corr. = 0.471) between the essentiality of Wsb2 and Bcl2l2 in PNS tumors (Fig. 5C). We verified these high through-put studies using a competitive growth assay to measure cell viability. First, we designed constitutively expressed shRNAs against Wsb2 and introduced them into the Neuroblastoma cell lines CHP134 and TGW. We employed three shRNAs against Wsb2. To verify the efficiency of these shRNAs, we performed qPCR in cells expressing each of the shRNAs (Fig. S5B). The cells were infected with a lentivirus encoding each shRNA and GFP, sorted 24h post-infection and mixed with an equal number of GFP negative cells (wild-type). The ratio of GFP-negative to GFP-positive cells was determined over a 3-day time course using FACS analysis. There was no significant shift in the ratio of cells expressing either control shRNA to the population of GFP-negative cells. In contrast, GFP-positive cells expressing shRNAs against Wsb2 were reduced in the population over time (Fig. 5D). To examine CHP134 cells lacking Wsb2 in isolation, we sorted GFP-positive cells 24h after infecting with each shRNA encoding virus and assessed the level of cleaved-PARP by western blot (Fig. 5E). We observed a clear induction of c-PARP in cells expressing an Wsb2 shRNA while no c-PARP could be observed in the control. To further examine this, we used the Caspase-glo assay in which a luminescent signal is emitted proportionally to caspase activity. Cells infected with shRNAs against WSB2 shows clear increased signal compared to control after normalization against non-infected cells (Fig. 5F). Taken together, our data are consistent with loss of Wsb2 causing cell death by initiating apoptosis in Neuroblastomas.

Discussion

A recent CRISPR screen found that Cul5 loss sensitized cells to inhibitors of Mcl1 and increased Bim and Noxa levels at both the protein and mRNA levels[55]. Additionally, findings from Hundley et al. showed that mutations of Arih2, Cul5, Rbx2 or Wsb2, sensitize HAP1 cells to the mitochondrial complex II inhibitor TTFA[41]. Moreover, high-throughput screening suggested synthetic lethality between Wsb2 mutation and Mcl1, March5, and Bcl-xl[42,43]. These studies suggest that loss of the $Cul5^{Wsb2}$ complex somehow primed cells for apoptosis, although it remained unclear if this was a direct effect.

Our study reveals that mutation of Cul5 or Wsb2 stabilizes $Bim_{EL,}$ Bim_L and, less dramatically, the more stable Bim_S isoform (Fig. 3A, B, C and S3A). Notably, Wsb2 recognizes these proteins through their association with the stable Bcl-xl and Mcl1 subunits. This redefines Bcl-xl's and Mcl1's long-known roles in Bim inhibition, showing that they function not only through sequestration, but also as a co-receptor with Wsb2 to target Bim. This mechanism operates alongside the well-characterized $SCF^{ß\text{-}TrCP1}$ pathway and reveals a broader regulatory role for anti-apoptotic BCL2 family members as substrate co-receptors for E3 ligases[19]. Finally, we demonstrate that Wsb2 is essential in Neuroblastoma cell lines and protects cells from apoptosis induction, highlighting its potential as a therapeutic target.

Several E3 ligases have been implicated in apoptosis regulation[56,57]. Bim is a known target of $SCF^{ßTrCP}$, and was also suggested to be regulated by Trim2 and $CRL2^{CIS}$ [58,59]. Similarly, other apoptotic proteins such as Bax, Bcl-xl or Noxa have been proposed to be regulated by Ibrdc2, Rnf183, and Cul5 respectively[60–63]. The pro-apoptotic Mcl1 was suggested to be targeted by March5/MULE; $SCF^{ß\text{-}TRCP}$,SCF^{FBW7} and Trim17[34,64–66]. However, in RPE1 cells, we find that Bcl-xl, Bcl2, Noxa and, to a lesser degree, Mcl1 are all stable (Fig. 3), suggesting that, unlike Bim, there may be little bulk turnover of these proteins in unperturbed normal cells. The $Cul5^{Wsb2\text{-}Bcl\text{-}xl/Mcl1}$ regulation of Bim is reminiscent of the observation that March5 ubiquitinates Mcl1 exclusively when Noxa and Mcl1 are in complex[64], showing the generality of Bcl2 family members acting as E3 ligases co-receptors.

Although Wsb2 depletion did not induce apoptosis in RPE1 cells, DepMap data revealed that peripheral nervous system (PNS) tumors, including neuroblastomas or malignant peripheral nerves sheath tumors (MPNSTs), are sensitive to Wsb2 depletion. Neuroblastomas are derived from primitive cells of the sympathetic nervous system and represent 15% of cancer death in children, with 90% of them diagnosed before the age of 5[67–71]. In aggressive Neuroblastoma, MYCN deregulation correlates with an upregulation of the p53 negative regulator Mdm2 as well as the anti-apoptotic factor Bcl2[71]. Overactivation of the MAPK/PI3K/Akt pathways by BDNF factor deregulation leads to a suppression of Bim induction and drug resistant tumors[71]. As such, our finding suggests that Cul5-Wsb2 inhibitors may adversely affect growth of Neuroblastomas irrespective of the BCL2 family member by causing strong up-regulation of Bim.

In this study we identified the $Cul5^{Wsb2\text{-}Bcl\text{-}xl/Mcl1}$ complex as a novel co-receptor for the regulation and degradation of Bim. Taking advantage of the powerful structure-based AlphaFold A.I[54], we identified the interaction motif required for Wsb2/Bcl-xl binding, which is essential for Bim targeting. While the K/R-E-M motif in Bcl-xl is shared by Bcl2 and Bcl-w it is not seen in Mcl1, and mutations in Wsb2 that disrupt Bcl-xl/Bim binding don't affect Mcl1/Bim binding. Thus, unlike many other E3s which recognize a common degron in a disparate set of substrates, Wsb2 recognizes functionally related substrates through independent mechanisms. Our results clearly indicate that the formation of the Bcl-xl-Bim or Mcl1-Bim dimers are necessary for Wsb2 interaction. We do not yet understand why Wsb2 fails to bind Bcl-xl alone, as Alphafold2 predicts this interaction to occur. Bcl-xl is known to undergo conformational changes in response to interactions with pro-apoptotic proteins, and these may be required for binding[72].

Figure Legends

Figure 1: Wsb2 and Cul5 mutants have high levels of Bim_{EL}, Bim_L and Bim_S.

A. Competitive growth assay comparing cells expressing sgRNAs against Wsb2 (red line) or control sgRNAs (blue line) in Cas9 positive HAP1 cells in the presence of 25 µM TTFA, over an 8-day period. **B**. Co-dependencies data from the DepMap consortium and Gene Ontology (GO) classification of the top 100 Wsb2's co-dependencies. **C**. Schematic representation of the intrinsic apoptotic pathway. **D**. Immunoblot analysis of apoptotic proteins in clonal RPE1 Wsb2 or Cul5 mutant cells. **E**. qPCR analysis of transcript levels of Mcl1, Bcl-xl, Bim_{EL}, and Noxa in Wsb2 or Cul5 mutant RPE1s cells normalized to WT. **F**. 5xHA-Wsb2 or an untagged Wsb2 allele were induced with DOX overnight and samples were immunoprecipitated with anti-HA antibodies.

Figure 2: Wsb2 regulates Bim through Bcl-xl and Mcl1

A. Schematic representation of the three main Bim splicing isoforms, highlighting their domains and regulatory sites and showing how phosphorylation events mediated by the MAPK pathway influence their stability and function. Specifically, Bim_{EL} is targeted for degradation by the $SCF^{\beta TrCP}$ complex following phosphorylation by Erk1/2 and Rsk1/2. Green lollipops indicate ubiquitination sites. Pink, orange, and purple lollipops represent Rsk1/2, Erk1/2, and Jnk/P38 phospho-sites, respectively. **B**. HA immunoprecipitation of extract from untagged or 5xHA-tagged Wsb2 cells co-expressing 3xFLAG tagged Bim_{EL}, Bim_L, or Bim_S after 3 hours DOX induction. **C**. HA immunoprecipitation of untagged or 5xHA-tagged Wsb2 in cells co-expressing or not expressing 3xFLAG tagged Bim_{EL}. **D.** HA immunoprecipitation from cells co-expressing 5xHA-Wsb2, 3xFLAG tagged Bim_{EL} or a truncated 3xFLAG-Bim lacking the C-terminal domain (3xFLAG-$Bim^{E2A\text{-}E4}$), as indicated. **E**. Same as Figure 2B, except that half the cells were treated with the pan-BH3 mimetic ABT-263 (Navitoclax) for 3 hours. **F**. Co-immunoblot analysis of 3xFLAG-Bim_L in the presence of the BH3 mimetics ABT-263, ABT-199, S63845, or A1331852. Immunoprecipitation

of 3xFlag-Bim was used to confirm the efficacy of each BH3 mimetic in disrupting its interaction (Fig. S2B) with the respective anti-apoptotic proteins. Dox (to induce 3Flag-Bim) and drugs were added for 3 hours before harvesting.

Figure 3: Wsb2 regulates Bim independently of the ßTrCP1 pathway

A. WT and Wsb2 mutant RPE1 cells were treated with cycloheximide and samples were harvested as indicated. **B.** As in panel A, except that PMA was added to one set of samples at the same time as cycloheximide. Quantitation (Fig. S3A), was normalized to Vinculin loading control and subsequently normalized to the t=0 signal. Phosphoforms of each Bim isoform were combined for normalization. **C.** As in panel B, comparing cells treated with Cycloheximide and ABT-263 to cells additionally treated with MLN4924. All drugs were added at t=0. **D**. WT and dox inducible 3xFLAG-Bim_{EL} RPE1 cells were DOX induced 3 hours and treated with Z-VAD-FMK (to block apoptosis) before treatment with cycloheximide and samples harvested as indicated. **E**. Flag-Ubiquitin and 13Myc-Bim_{L} were co-induced with DOX in wild type or Wsb2 mutant RPE1 cells as indicated, and extracts were immunoprecipitated with anti-Myc antibodies.

Figure 4: Bim is targeted through a direct Wsb2-Bcl-xl interaction

A. Alphafold 2 multimer predicted Wsb2 dimerization with BCL2 protein family members. The four metrics iPTM (Confidence of protein-protein interaction), PTM (Accuracy of the relative positioning of domains within a multi-domain protein), pLDDT (Confidence in the local structure) and PAE (Expected positional error in the distance between pairs of residues) are shown for dimer prediction between Wsb2 and apoptosis proteins. The Cul5 adaptors EloB and EloC were used as a positive control. **B**. Top panel represent Alphafold2 predicted structure of the Wsb2/Bcl-xl complex with pLDDT coloring. Bottom panel with arbitrary coloring represent Alphafold2 predicted interaction between Wsb2 and Bcl-xl through the yellow and light blue residues. **C**. Alignment of Bcl-xl, Bcl2, Bcl-w, Mcl1 and Bim showing conservation of the interaction motif between Bcl-xl, Bcl2 and Bcl-w, framed in red. **D**. *In vivo* validation of Alphafold2 dimer predictions was performed using co-immunoprecipitation assays. A 5xHA-tagged Wsb2 allele was co-expressed with either V5-tagged wild-type Bcl-xl or Bcl-$xl^{K157A/E158A/M159A}$ as indicated. In all cell lines, a 3xFlag-tagged Bim_{EL} allele was co-expressed. **E**. HA immunoprecipitation in cell lines expressing a 5HA-tagged WT or $Wsb2^{R157E/R174E/R297E}$ allele and a V5-tagged wild-type Bcl-xl, as indicated. In all cell lines, a 3xFlag-tagged Bim_{EL} allele was co-expressed. **F.** HA immunoprecipitation in cells expressing an untagged Wsb2, 5HA-tagged Wsb2 or 5HA-tagged $Wsb2^{R157E/R174E/R297E}$ allele. In all cell lines, a 3xFlag-tagged Bim_{EL} allele was co-expressed.

Figure 5: Wsb2 is essential in Neuroblastoma

A. GTEx portal analysis of transcript levels in bulk tissue RNA sequencing for Wsb2, Wsb1, EloB, and EloC. **B**. DepMap data of tumor sensitivity to Wsb2 depletion across multiple cancer type. **C**. DepMap data correlation of tumor sensitivity to Wsb2 and Bcl2l2 depletion. **D**. Time course competitive growth assay of CHP134 or TGW cells expressing shRNA against Wsb2. Wild-type (GFP-) cells were mixed at an equal ratio with cells expressing either a shRNA scramble control (GFP+) or a shRNA targeting Wsb2 (GFP+). The ratio of GFP-positive to GFP-negative cells was measured over 3 days and normalized to a GFP-negative wild-type control signal. Data are represented as mean ± SD **E**. Immunoblot analysis in CHP134 cells expressing Wsb2 shRNA, showing that Wsb2 depletion leads to increased levels of cleaved Parp (c-Parp). **F**. Promega Caspase-Glo assay luminescence signal normalized to 1000 cells and uninfected control, after transfection with shRNAs against WSB2 or Control over a 2-day time course. Data are represented as mean ± Range.

Supplemental Information

Figure S1: Wsb2 clone sequencing validation and sensitivity to mitochondrial stressors
A. ICE analysis results of Sanger sequencing results from the Wsb2 CRISPR clone generated for this study **B.** Immunoblot of Wild-type and Wsb2 mutant cell extract following treatment with Rotenone or Camptothecine for 72h.

Figure S2: Wsb2 doesn't directly interact with Bcl-w and Bcl2

A. As figure 2D, except cell extract were blotted for Bcl2 and Bcl-w **B.** Co-immunoblot analysis of 3xFLAG-Bim_L in the presence of the BH3 mimetics ABT-263, ABT-199, S63845, or A1331852. Immunoprecipitation of 3xFlag-Bim was used to confirm the efficacy of each BH3 mimetic in disrupting its interaction with the respective anti-apoptotic proteins.

Figure S3: Quantification of CHX/PMA treatment
A. Quantification of WT and Wsb2 mutant RPE1 cells from 2 immunoblots following treatment with cycloheximide with or without PMA added to one set of samples at the same time as cycloheximide. Signals were normalized to vinculin loading control and subsequently normalized to the t=0 signal. Phosphoforms of each Bim isoforms were combined for normalization. **B.** Western blot analysis of Borzetomib and MG132 effects on 5xHA-Wsb2 and 3xFLAG-Bim_{EL} expression compared to untreated.

Figure S4: Alphafold2 MM plots
A. Alphafold 2 multimer predicted Wsb1 dimerization with BCL2 protein family members scores. The Cul5 substrate adaptors EloB and EloC were used as a positive control. **B.** Alphafold 2 multimer predicted Wsb2 dimerization with Bcl-xl DKEM motif mutants scores. Right Panel represent a zoomed in window of the upper right cluster of predicted interaction in the left panel

Figure S5: DepMap statistics & shRNA controls
A. DepMap generated regression line for Peripheral Nervous System (PNS) tumors and all other tumors types (referred to as not PNS) for sensitivity to Wsb2 versus Bcl2l2 depletion **B.** Quantitative PCR of Wsb2 transcript levels. Constitutive expression of a Wsb2 targeting shRNA in RPE1 or CHP134 cells decrease Wsb2 transcript level compared to scramble. Data are represented as mean ± SD

Materials & Methods

Cell Culture

Cell Lines
Cell lines were maintained using standard tissue culture techniques. HEK293T and RPE1 were cultured in DMEM F/12 (Thermofisher #11320082) with 10% heat inactivated Fetal Bovine Serum (Gibco #A52568-01) and 1X Anti-Anti (Gibco #15240-062). HAP1 were cultured in IMDM (Thermofisher # 12-440-061) with 10% heat inactivated Fetal Bovine Serum and 1X Anti-Anti. CHP134 were cultured in RPMI (Thermofisher #21870-076), 2mM L-glutamine (Sigma-Aldrich #SLCQ1268), 20% heat inactivated Fetal Bovine Serum and 1X Anti-Anti. TGW were cultured in EMEM (Corning #10-009-CV) with 20% heat inactivated Fetal Bovine Serum and 1X Anti-Anti. All cells grew at 37°C with 5% CO2.

Lentiviral particle generation & transduction
Lentiviral particles were produced using HEK293T seeded at ~6x10^5 cells into a 6-well plate (~30-40% confluency) and transfected the following day (~80% confluency) with 1 µg of the vector of interest, 750 ng pSPAX2, 250 ng VSVG, and 6 µL Fugene® HD (Promega #E2311) in 100 µL Opti-MEM® (Gibco #31985-070). The transfection mix was incubated 15 minutes at RT and added dropwise to cells. After 6 hours at 37°C, the medium was replaced with fresh media. Virus-containing supernatants were collected after 24 hours, filtered (0.45 µm, Thermo Scientific #723-2545), and stored at -80°C. Target cells were transduced with a 1:10 dilution of virus-containing media in the presence of 5 µg/mL Polybrene or 8 µg/mL Protamine Sulfate.

Cell lines generation
RPE1 clonal lines were generated by sequential lentiviral transduction with plasmids carrying DOX-inducible CRISPR-Cas9 systems targeting CUL5 or WSB2 (gRNA sequences: CUL5 - ACTATCTTAGCTGAGTGCCA, WSB2 - CACGTTAATTCGGAAGCTAG; Toronto CRISPR Human Knockout Library, TKOv3). Cells were selected in 1 µg/mL or 10 µg/mL puromycin, induced with 1 µg/mL doxycycline for 3 days, and sorted into single-cell clones by FACS. Clones were validated by western blotting (Cul5) or sequencing (Wsb2) (Fig. S1A).

Method details

Time Course Experiments

Drugs concentration used outside of sensitivity assay are 10uM ABT-263 Selleck Chemicals #S1001 ; 500nM A-1331852 Selleck Chemicals #S7801 ; 15uM S63845 TargetMol #T5346 ; 15uM ABT-199 TargetMol #T2119 ; Cycloheximide 50uM Sigma-Aldrich #C4859-1ML ; 100nM phorbol 12-myristate 13-acetate (PMA) MCE #HY-18739 ; 500 nM MLN4924 MedChem Express #HY-70062 ; 50-100uM Z-VAD-FMK AdooQ BioScience #A12373

qPCR Analysis

Total RNA was extracted from 10^5–10^7 cells using TRIzol (ThermoFisher #15596018) according to the manufacturer's protocol, purified, and DNase I-treated using the RNA Clean & Concentrator™-5 Kit (Zymo Research #R1015). RNA purity was confirmed by nanodrop quantification and/or agarose gel electrophoresis. 5ug of RNA were reverse-transcribed using the Tetro RT-PCR Kit (Meridian Bioscience #BIO-65043). Primers (75–150 bp, exon-exon junctions when possible) were designed using NCBI Primer-BLAST and validated with standard curves (5×10-fold dilutions). Relative expression levels were normalized using the ΔΔCt method with Actin as the housekeeping gene. Primer sequences are:
•**CUL5**: Forward: GCAAGCACAGGCACGAGT; Reverse: TTGCTGCCCTGTTTACCCAT
•**WSB2**: Forward: CTGAGGTCACTCCACCACAC; Reverse: GGAGTCTGTCATCTGCCACC
•**BIM**: Forward: ATGTCTGACTCTGACTCTCG; Reverse: CCTTGTGGCTCTGTCTGTAG
•**NOXA**: Forward: AGAGCTGGAAGTCGAGTGTG; Reverse: GAAACGTGCACCTCCTGAGA
•**MCL1**: Forward: GTTTTCAGCGACGGCGTAAC; Reverse: CTCCACAAACCCATCCCAGC
•**BCLXL**: Forward: TCAATGGCAACCCATCCTGG; Reverse: GAGCTGGGATGTCAGGTCAC
•**ACTIN**: Forward: AGGCACCAGGGGGTGAT; Reverse: GCCCACATAGGAATCCTTCTGAC

Western Blotting

Protein extraction
Proteins were extracted by resuspension and mechanical lysis in lysis buffer (50% 2X RIPA buffer (100mM Tris pH8; 300mM NaCl; 2% TritonX100; 1% Sodium Deoxycholate; 0,2% SDS); 80mM Beta-Glycerophosphate; 5mM NaF; PepA; Protein Inhibitor cocktail; 2mM Sodium orthovanadate; 1mM PMSF or 50% 2X RIPA buffer; cOmplete Tablets, Mini EDTA-free, *EASYpack* (Roche #04693159001) and PhosSTOP *EASYpack* (Roche #04906837001) following manufacturer recommendation). After 30 minutes on ice, lysates were clarified by centrifugation at 21,000 × g for 15 minutes at 4 °C. Protein concentrations were determined via BCA assay, then normalized lysates were mixed with Laemmli buffer (50 mM DTT) and heated at 95 °C for 5 minutes.

SDS-AGE and transfer
Proteins were loaded at equal quantity on Criterion 26- or 18-wells TGX 4-20% Precast polyacrylamide gel (BIORAD #5671095; #5671094) and ran at constant Amperage in Running buffer (384mM Glycine; 50mM Tris-Base; 0.1% SDS(w/v)). The proteins were subsequently transferred to a 0.2uM Nitrocellulose blotting membrane (Amersham Protan #10600001) at constant amperage; 100V for 1h at 4°C using a BIORAD PowerPack HC, in transfer buffer (20mM Tris-Base; 150mM Glycine; 0,0374% SDS (w/v); 2% Methanol (v/v)). Membranes were subsequently blocked in PBS-T (0.05% Tween) 5% milk for 1h at RT and incubated overnight with primary antibodies.

Detection method
Membranes were washed 3 times in PBS-T (0.05% Tween) for 5 minutes each time before being incubated with secondary HRP antibody for 1h at RT in PBS-T (0.05% tween) 5% Milk. Membranes were subsequently washed 3 times in PBS-T for 5 minutes each time. Proteins were revealed by incubating the membrane with regular or strong ECL (PROMETHEUS #20-300B or ThermoScientific #34096), depending on the signal quality, for 2 minutes at RT before imaging protein signal on a LICOR Odyssey. Protein signal quantification was performed using the ImageStudio LICOR software and Microsoft Excel.

Immunoprecipitation/Co-immunoprecipitation

Cells were resuspended in lysis buffer (150 mM NaCl, 50 mM Tris pH 8, 0.5% Triton X-100) supplemented with PhosStop™ phosphatase and cOmplete™ protease inhibitors. Lysates were prepared by passing them 10 times through a 21-gauge needle, then incubated for 30 minutes at 4 °C with rotation and cleared by centrifugation at 21,000 × g at 4°C for 20 minutes. Protein concentrations were measured by BCA assay. For HA-tag IP, lysates were incubated 30 minutes at RT with anti-HA–coated beads (Pierce or Dynabeads Protein A preloaded with anti-HA). For FLAG-tag IP, lysates were incubated 30 minutes (or 1 hour for ubiquitin IP) with anti-DYKDDDDK beads. For V5-tag IP, lysates were pre-incubated with anti-V5 antibodies, then with Dynabeads. For Myc-tag IP, lysates were incubated 1 hour at RT with anti-c-Myc beads and washed in 50% 2× RIPA. Proteins were eluted at 65 °C for 10 minutes, reduced in Laemmli buffer with 50 mM DTT, and heated to 95 °C for 5 minutes before western blotting.

Alphafold Analysis

Protein FASTA sequences were obtained on the Uniprot database. Default settings were used for collabfold version 1.5.5. To evaluate the accuracy of our protein complex model predictions, we used the four parameters used by AlphaFold2 for predicted model confidence, PTM, iPTM, pLDDT, PAE. We considered iPTM > 0.8; PTM > 0.5; PAE < 10 and pLDDT > 77 to be significant.

Internally controlled, competitive growth assays

shRNA constructs targeting WSB2 were ordered as pre-designed (Sigma-Aldrich) or synthesized (IDT) and cloned into the pLKO.1 vector. shRNAs lentiviral constructs (GFP^+) were used to transfect cells, which were then sorted by FACS (SonySH800). The GFP^+ fraction was mixed 1:1 with an untransfected GFP^- population in RPMI (20% FBS, 1x Anti-Anti, 2 mM L-Glutamine) or EMEM (20% FBS, 1x Anti-Anti) at T0. Each day, 3,500–10,000 cells per condition were resorted to quantify the GFP^+/GFP^- ratio using a 99th-percentile gating strategy. The resulting ratios were normalized to the T0 value. The mean of each experiment was pooled and represented as bar graphs ± SD. The shRNAs sequences are: (sh1) CACGGCTTCTTACGATACCAA; (sh2) CCCTTCGAAGTTTCCTAACAA; (sh3) CCCACCAGTTTGATTGGAAGT; (shCTRL1) CAACAAGATGAAGAGCACCAA; (shCTRL2) CCTAAGGTTAAGTCGCCCTCG.

Caspase-Glo Assay

At the starting point of the experiment (T0), 1200 viable, singlets wild-type (pre-infection) CHP134 cells were sorted by FACS and serially diluted in a 3-points 10-fold dilution series in a final volume of 25ul per well in a white-walled 96 multiwell Corning® Microplates (Cat.# 3917). According to manufacturer instructions, an equal volume of Caspase-Glo® reagent was added to each well, followed by a 30 minutes incubation at RT on a rotator, protected from light. Luminescent signal was subsequently measured using a Synergy II plate reader. After transfection, 1200 viable, singlets GFP+ CHP134 cells were sorted by FACS for each shRNA and wild-type control and processed identically. We used 1000 cells for our experiments, as such the luminescent signal was normalized to the number of cells and then to the wild-type control (used for that particular day) to assess apoptosis level. The mean of each experiment were pooled and represented as bar graphs ± Range.

Antibodies for Western Blotting

1:500 CUL5 (#sc-373822), 1:1000 EloC (#sc-135895), 1:1000 PUMA (#4976S), 1:1000 NOXA (#14766S), 1:1000 BIK (#4592T), 1:1000 BAD (#9292S), 1:1000 BCL2 (#4223S), 1:1000 BCL-w (#2724S), 1:1000 BCLxL (#2764S), 1:1000 MCL1 (#94296S), 1:1000 BID (#2002T), 1:1000 BAK (#12105S), 1:1000 BAX (#5023S), 1:1000 BIM (#2933S), 1:1000 P53 (#9282S), 1:1000 HA (#3724S), 1:1000 FLAG (#14793S), 1:1000 MYC (#2276S), 1:1000 V5 (#13202S), 1:1000 MARCH5 (#v06-1036), 1:500 Cyclin D1 (#ab16663), 1:3000 ACTIN (#A5441-100UL), 1:3000 VINCULIN (#V9131).

Acknowledgments

We thank the UCSF Helen Diller Family Comprehensive Cancer Center LCA and LCA-Genomic Core Facility for the service they provided in support of this research. We extend our thanks to Emma Bolech and Candace S.Y Chan for their contributions to this project. We also appreciate the Weiss laboratory for providing the Neuroblastoma

CHP134 cell line with special thanks to Hiroyuki Yoda for his assistance. This research was supported by funding from the Resource Allocation Program (REAC), the PBBR Program, the Cancer League, and the NIH (R35GM118104).

Author Contributions

DPT: Conceptualization, Methodology, Writing – original draft, Funding acquisition, Supervision, Resources, Project administration, Writing – review & editing
WVZ: Conceptualization, Methodology, Writing – original draft, Investigation, Formal analysis, Validation, Data curation, Visualization, Writing – review & editing
EMCA: Investigation, Validation
NG: Investigation

Competing Interest Statement

The authors declare no financial or non-financial competing interests in relation to this work

References

1. Yuan, J. & Ofengeim, D. A guide to cell death pathways. *Nat. Rev. Mol. Cell Biol.* **25**, 379–395 (2024).
2. Naim, S. & Kaufmann, T. The Multifaceted Roles of the BCL-2 Family Member BOK. *Front. Cell Dev. Biol.* **8**, (2020).
3. Westphal, D., Kluck, R. M. & Dewson, G. Building blocks of the apoptotic pore: how Bax and Bak are activated and oligomerize during apoptosis. *Cell Death Differ.* **21**, 196–205 (2014).
4. Green, D. R. The Mitochondrial Pathway of Apoptosis Part II: The BCL-2 Protein Family. *Cold Spring Harb. Perspect. Biol.* **14**, a041046 (2022).
5. Qian, S. *et al.* The role of BCL-2 family proteins in regulating apoptosis and cancer therapy. *Front. Oncol.* **12**, (2022).
6. Czabotar, P. E. *et al.* Bax Crystal Structures Reveal How BH3 Domains Activate Bax and Nucleate Its Oligomerization to Induce Apoptosis. *Cell* **152**, 519–531 (2013).
7. Kim, H. *et al.* Hierarchical regulation of mitochondrion-dependent apoptosis by BCL-2 subfamilies. *Nat. Cell Biol.* **8**, 1348–1358 (2006).
8. Letai, A. *et al.* Distinct BH3 domains either sensitize or activate mitochondrial apoptosis, serving as prototype cancer therapeutics. *Cancer Cell* **2**, 183–192 (2002).
9. Dai, H., Pang, Y.-P., Ramirez-Alvarado, M. & Kaufmann, S. H. Evaluation of the BH3-only Protein Puma as a Direct Bak Activator*. *J. Biol. Chem.* **289**, 89–99 (2014).
10. Dai, H. *et al.* Transient binding of an activator BH3 domain to the Bak BH3-binding groove initiates Bak oligomerization. *J. Cell Biol.* **194**, 39–48 (2011).
11. Nakagawa, T. *et al.* EGFR-TKI Resistance Due to BIM Polymorphism Can Be Circumvented in Combination with HDAC Inhibition. *Cancer Res.* **73**, 2428–2434 (2013).
12. Ng, K. P. *et al.* A common BIM deletion polymorphism mediates intrinsic resistance and inferior responses to tyrosine kinase inhibitors in cancer. *Nat. Med.* **18**, 521–528 (2012).
13. Tanimoto, A. *et al.* Histone Deacetylase 3 Inhibition Overcomes BIM Deletion Polymorphism–Mediated Osimertinib Resistance in EGFR-Mutant Lung Cancer. *Clin. Cancer Res.* **23**, 3139–3149 (2017).
14. Gagné, V. *et al.* Bim Polymorphisms: Influence on Function and Response to Treatment in Children with Acute Lymphoblastic Leukemia. *Clin. Cancer Res.* **19**, 5240–5249 (2013).
15. Yu, M. *et al.* The BIM deletion polymorphism potentiates the survival of leukemia stem and progenitor cells and impairs response to targeted therapies. *Leukemia* 1–10 (2024) doi:10.1038/s41375-024-02418-0.
16. Eleveld, T. F. *et al.* MEK inhibition causes BIM stabilization and increased sensitivity to BCL-2 family member inhibitors in RAS-MAPK-mutated neuroblastoma. *Front. Oncol.* **13**, (2023).
17. Sionov, R. V., Vlahopoulos, S. A. & Granot, Z. Regulation of Bim in Health and Disease. *Oncotarget* **6**, 23058–23134 (2015).
18. O'Connor, L. *et al.* Bim: a novel member of the Bcl-2 family that promotes apoptosis. *EMBO J.* **17**, 384–395 (1998).
19. Dehan, E. *et al.* βTrCP- and Rsk1/2-mediated degradation of BimEL inhibits apoptosis. *Mol. Cell* **33**, 109–116 (2009).
20. Lin, C. P. & Komives, E. A. Diversity of structure and function in Cullin E3 ligases. *Curr. Opin. Struct. Biol.* **88**, 102879 (2024).

21. Lydeard, J. R., Schulman, B. A. & Harper, J. W. Building and remodelling Cullin–RING E3 ubiquitin ligases. *EMBO Rep.* **14**, 1050–1061 (2013).
22. Harper, J. W. & Schulman, B. A. Cullin-RING Ubiquitin Ligase Regulatory Circuits: A Quarter Century Beyond the F-Box Hypothesis. *Annu. Rev. Biochem.* **90**, 403–429 (2021).
23. Bennett, E. J., Rush, J., Gygi, S. P. & Harper, J. W. Dynamics of Cullin-RING Ubiquitin Ligase Network Revealed by Systematic Quantitative Proteomics. *Cell* **143**, 951–965 (2010).
24. Okumura, F., Joo-Okumura, A., Nakatsukasa, K. & Kamura, T. The role of cullin 5-containing ubiquitin ligases. *Cell Div.* **11**, 1 (2016).
25. Babon, J. J., Sabo, J. K., Zhang, J.-G., Nicola, N. A. & Norton, R. S. The SOCS Box Encodes a Hierarchy of Affinities for Cullin5: Implications for Ubiquitin Ligase Formation and Cytokine Signalling Suppression. *J. Mol. Biol.* **387**, 162–174 (2009).
26. Zhao, Y., Xiong, X. & Sun, Y. Cullin-RING Ligase 5: Functional characterization and its role in human cancers. *Semin. Cancer Biol.* **67**, 61–79 (2020).
27. Scott, D. C. *et al.* Two Distinct Types of E3 Ligases Work in Unison to Regulate Substrate Ubiquitylation. *Cell* **166**, 1198-1214.e24 (2016).
28. Kelsall, I. R. *et al.* TRIAD1 and HHARI bind to and are activated by distinct neddylated Cullin-RING ligase complexes. *EMBO J.* **32**, 2848–2860 (2013).
29. Kostrhon, S. *et al.* CUL5-ARIH2 E3-E3 ubiquitin ligase structure reveals cullin-specific NEDD8 activation. *Nat. Chem. Biol.* **17**, 1075–1083 (2021).
30. Rape, M. Ubiquitylation at the crossroads of development and disease. *Nat. Rev. Mol. Cell Biol.* **19**, 59–70 (2018).
31. Duan, S. & Pagano, M. Ubiquitin ligases in cancer: functions and clinical potentials. *Cell Chem. Biol.* **28**, 918–933 (2021).
32. Welcker, M. & Clurman, B. E. FBW7 ubiquitin ligase: a tumour suppressor at the crossroads of cell division, growth and differentiation. *Nat. Rev. Cancer* **8**, 83–93 (2008).
33. Senft, D., Qi, J. & Ronai, Z. A. Ubiquitin ligases in oncogenic transformation and cancer therapy. *Nat. Rev. Cancer* **18**, 69–88 (2018).
34. Inuzuka, H. *et al.* SCFFBW7 regulates cellular apoptosis by targeting MCL1 for ubiquitylation and destruction. *Nature* **471**, 104–109 (2011).
35. Yen, H.-C. S., Xu, Q., Chou, D. M., Zhao, Z. & Elledge, S. J. Global protein stability profiling in mammalian cells. *Science* **322**, 918–923 (2008).
36. Mark, K. G., Simonetta, M., Maiolica, A., Seller, C. A. & Toczyski, D. P. Ubiquitin Ligase Trapping Identifies an SCFSaf1 Pathway Targeting Unprocessed Vacuolar/Lysosomal Proteins. *Mol. Cell* **53**, 148–161 (2014).
37. Suiter, C. C. *et al.* Combinatorial mapping of E3 ubiquitin ligases to their target substrates. *Mol. Cell* **85**, 829-842.e6 (2025).
38. Benanti, J. A., Cheung, S. K., Brady, M. C. & Toczyski, D. P. A proteomic screen reveals SCFGrr1 targets that regulate the glycolytic–gluconeogenic switch. *Nat. Cell Biol.* **9**, 1184–1191 (2007).
39. Cory, S. & Adams, J. M. The Bcl2 family: regulators of the cellular life-or-death switch. *Nat. Rev. Cancer* **2**, 647–656 (2002).
40. Loo, L. S. W. *et al.* BCL-xL/BCL2L1 is a critical anti-apoptotic protein that promotes the survival of differentiating pancreatic cells from human pluripotent stem cells. *Cell Death Dis.* **11**, 1–18 (2020).
41. Hundley, F. V. *et al.* A comprehensive phenotypic CRISPR-Cas9 screen of the ubiquitin pathway uncovers roles of ubiquitin ligases in mitosis. *Mol. Cell* **81**, 1319-1336.e9 (2021).
42. DeWeirdt, P. C. *et al.* Genetic screens in isogenic mammalian cell lines without single cell cloning. *Nat. Commun.* **11**, 752 (2020).
43. DeWeirdt, P. C. *et al.* Optimization of AsCas12a for combinatorial genetic screens in human cells. *Nat. Biotechnol.* **39**, 94–104 (2021).
44. Jha, R. K., Kouzine, F. & Levens, D. MYC function and regulation in physiological perspective. *Front. Cell Dev. Biol.* **11**, (2023).
45. Aubrey, B. J., Kelly, G. L., Janic, A., Herold, M. J. & Strasser, A. How does p53 induce apoptosis and how does this relate to p53-mediated tumour suppression? *Cell Death Differ.* **25**, 104–113 (2018).
46. Lu, K. *et al.* Multiple cullin-associated E3 ligases regulate cyclin D1 protein stability. *eLife* **12**, e80327 (2023).
47. Behera, A., Panigrahi, G. K. & Sahoo, A. Nonsense-Mediated mRNA Decay in Human Health and Diseases: Current Understanding, Regulatory Mechanisms and Future Perspectives. *Mol. Biotechnol.* (2024) doi:10.1007/s12033-024-01267-7.

48. Jiao, D. *et al.* Disruption of WSB2-mediated NOXA Degradation Induces Synthetic Lethality to Anti-apoptotic BCL-2 Family Protein Inhibitors. *eLife* **13**, (2024).
49. Shao, S., Cui, D., Zheng, C., Xiong, X. & Zhao, Y. WSB2 inhibits apoptosis and autophagy by targeting NOXA for degradation. *MedComm* **6**, e70071 (2025).
50. Chi, X. *et al.* The carboxyl-terminal sequence of bim enables bax activation and killing of unprimed cells. *eLife* **9**, e44525 (2020).
51. Wiggins, C. M. *et al.* BIMEL, an intrinsically disordered protein, is degraded by 20S proteasomes in the absence of poly-ubiquitylation. *J. Cell Sci.* **124**, 969–977 (2011).
52. Warr, M. R. *et al.* BH3-ligand regulates access of MCL-1 to its E3 ligase. *FEBS Lett.* **579**, 5603–5608 (2005).
53. Conage-Pough, J. E. & Boise, L. H. Phosphorylation alters Bim-mediated Mcl-1 stabilization and priming. *FEBS J.* **285**, 2626–2640 (2018).
54. Jumper, J. *et al.* Highly accurate protein structure prediction with AlphaFold. *Nature* **596**, 583–589 (2021).
55. Kabir, S. *et al.* The CUL5 ubiquitin ligase complex mediates resistance to CDK9 and MCL1 inhibitors in lung cancer cells. *eLife* **8**, e44288.
56. Abbas, R. & Larisch, S. Killing by Degradation: Regulation of Apoptosis by the Ubiquitin-Proteasome-System. *Cells* **10**, 3465 (2021).
57. Roberts, J. Z., Crawford, N. & Longley, D. B. The role of Ubiquitination in Apoptosis and Necroptosis. *Cell Death Differ.* **29**, 272–284 (2022).
58. Zhang, W. *et al.* RACK1 and CIS Mediate the Degradation of BimEL in Cancer Cells *. *J. Biol. Chem.* **283**, 16416–16426 (2008).
59. Thompson, S. *et al.* Identification of a Novel Bcl-2-interacting Mediator of Cell Death (Bim) E3 Ligase, Tripartite Motif-containing Protein 2 (TRIM2), and Its Role in Rapid Ischemic Tolerance-induced Neuroprotection*. *J. Biol. Chem.* **286**, 19331–19339 (2011).
60. Benard, G. *et al.* IBRDC2, an IBR-type E3 ubiquitin ligase, is a regulatory factor for Bax and apoptosis activation. *EMBO J.* **29**, 1458–1471 (2010).
61. Wu, Y. *et al.* Transmembrane E3 ligase RNF183 mediates ER stress-induced apoptosis by degrading Bcl-xL. *Proc. Natl. Acad. Sci. U. S. A.* **115**, E2762–E2771 (2018).
62. Xu, S. *et al.* Cullin-5 neddylation-mediated NOXA degradation is enhanced by PRDX1 oligomers in colorectal cancer. *Cell Death Dis.* **12**, 265 (2021).
63. Zhou, W. *et al.* Neddylation E2 UBE2F promotes the survival of lung cancer cells by activating CRL5 to degrade NOXA via the K11 linkage. *Clin. Cancer Res. Off. J. Am. Assoc. Cancer Res.* **23**, 1104–1116 (2017).
64. Arai, S. *et al.* MARCH5 mediates NOXA-dependent MCL1 degradation driven by kinase inhibitors and integrated stress response activation. *eLife* **9**, e54954 (2020).
65. Magiera, M. M. *et al.* Trim17-mediated ubiquitination and degradation of Mcl-1 initiate apoptosis in neurons. *Cell Death Differ.* **20**, 281–292 (2013).
66. Ding, Q. *et al.* Degradation of Mcl-1 by β-TrCP Mediates Glycogen Synthase Kinase 3-Induced Tumor Suppression and Chemosensitization. *Mol. Cell. Biol.* **27**, 4006–4017 (2007).
67. Esiashvili, N., Anderson, C. & Katzenstein, H. M. Neuroblastoma. *Curr. Probl. Cancer* **33**, 333–360 (2009).
68. NCCR*Explorer Application. https://nccrexplorer.ccdi.cancer.gov/application.html.
69. Brodeur, G. M. Neuroblastoma: biological insights into a clinical enigma. *Nat. Rev. Cancer* **3**, 203–216 (2003).
70. Park, J. R., Eggert, A. & Caron, H. Neuroblastoma: biology, prognosis, and treatment. *Hematol. Oncol. Clin. North Am.* **24**, 65–86 (2010).
71. Qiu, B. & Matthay, K. K. Advancing therapy for neuroblastoma. *Nat. Rev. Clin. Oncol.* **19**, 515–533 (2022).
72. Vasquez-Montes, V., Kyrychenko, A., Vargas-Uribe, M., Rodnin, M. V. & Ladokhin, A. S. Conformational Switching in Bcl-xL: Enabling Non-Canonic Inhibition of Apoptosis Involves Multiple Intermediates and Lipid Interactions. *Cells* **9**, 539 (2020).

A

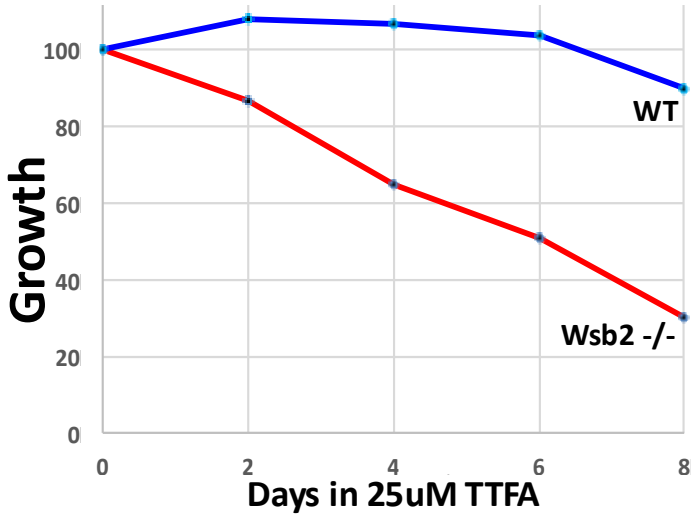
Growth
100
80
60
40
20
0
0
2
4
6
8
Days in 25uM TTFA
WT
Wsb2 -/-

B

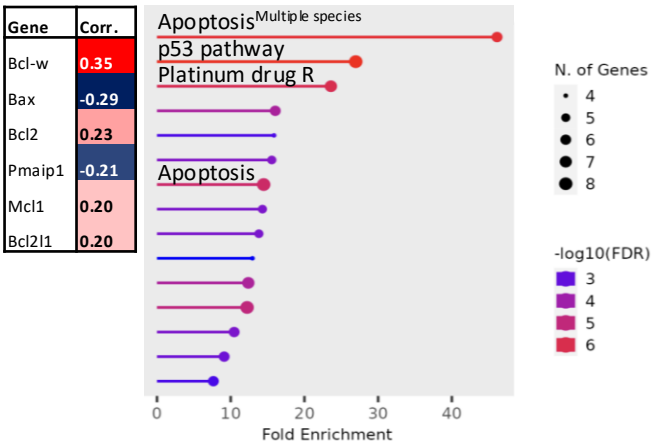
Gene
Corr.
Bcl-w
0.35
Bax
-0.29
Bcl2
0.23
Pmaip1
-0.21
Mcl1
0.20
Bcl2l1
0.20
Apoptosis Multiple species
p53 pathway
Platinum drug R
Apoptosis
0
10
20
30
40
Fold Enrichment
N. of Genes
4
5
6
7
8
-log10(FDR)
3
4
5
6

C

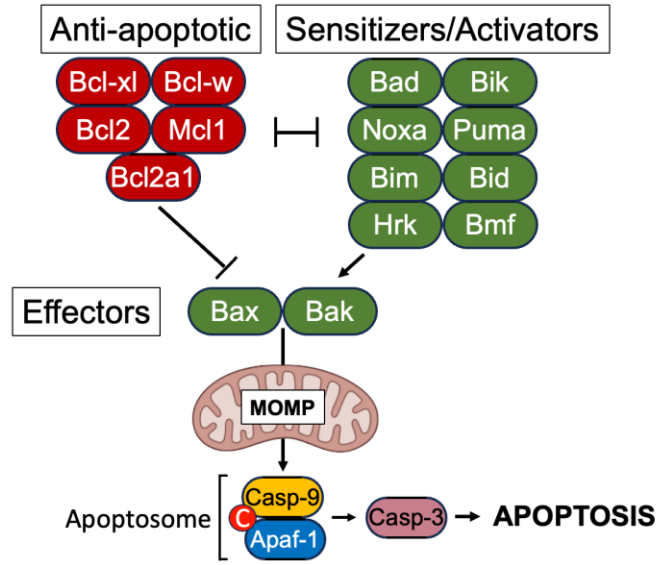
Anti-apoptotic
Sensitizers/Activators
Bcl-xl
Bcl-w
Bcl2
Mcl1
Bcl2a1
Bad
Bik
Noxa
Puma
Bim
Bid
Hrk
Bmf
Effectors
Bax
Bak
MOMP
Apoptosome
Casp-9
C
Apaf-1
Casp-3
APOPTOSIS

D

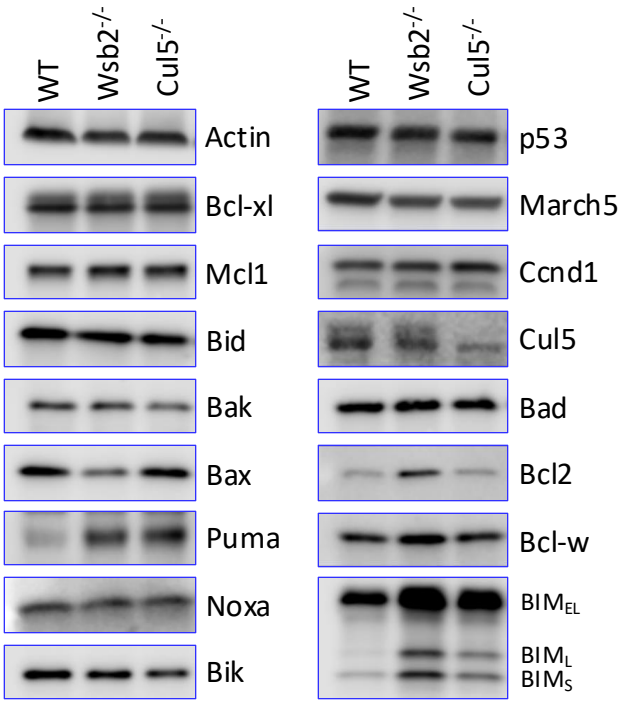
WT
Wsb2-/-
Cul5-/-
Actin
Bcl-xl
Mcl1
Bid
Bak
Bax
Puma
Noxa
Bik
p53
March5
Ccnd1
Cul5
Bad
Bcl2
Bcl-w
BIMEL
BIML
BIMS

E

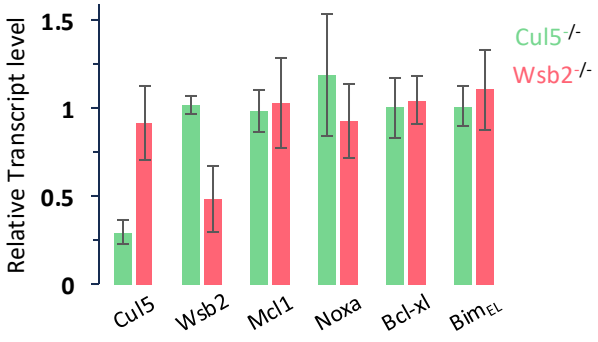
Relative Transcript level
1.5
1
0.5
0
Cul5-/-
Wsb2-/-
Cul5
Wsb2
Mcl1
Noxa
Bcl-xl
BimEL

F

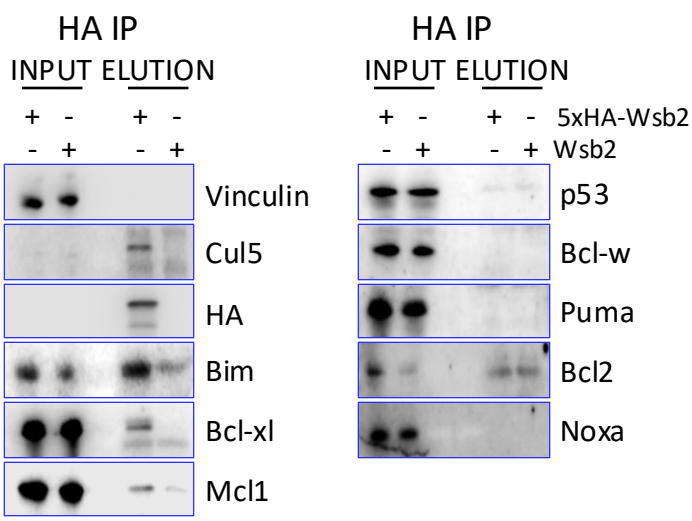
HA IP
INPUT ELUTION
+ - + -
- + - +
Vinculin
Cul5
HA
Bim
Bcl-xl
Mcl1
HA IP
INPUT ELUTION
+ - + - 5xHA-Wsb2
- + - + Wsb2
p53
Bcl-w
Puma
Bcl2
Noxa

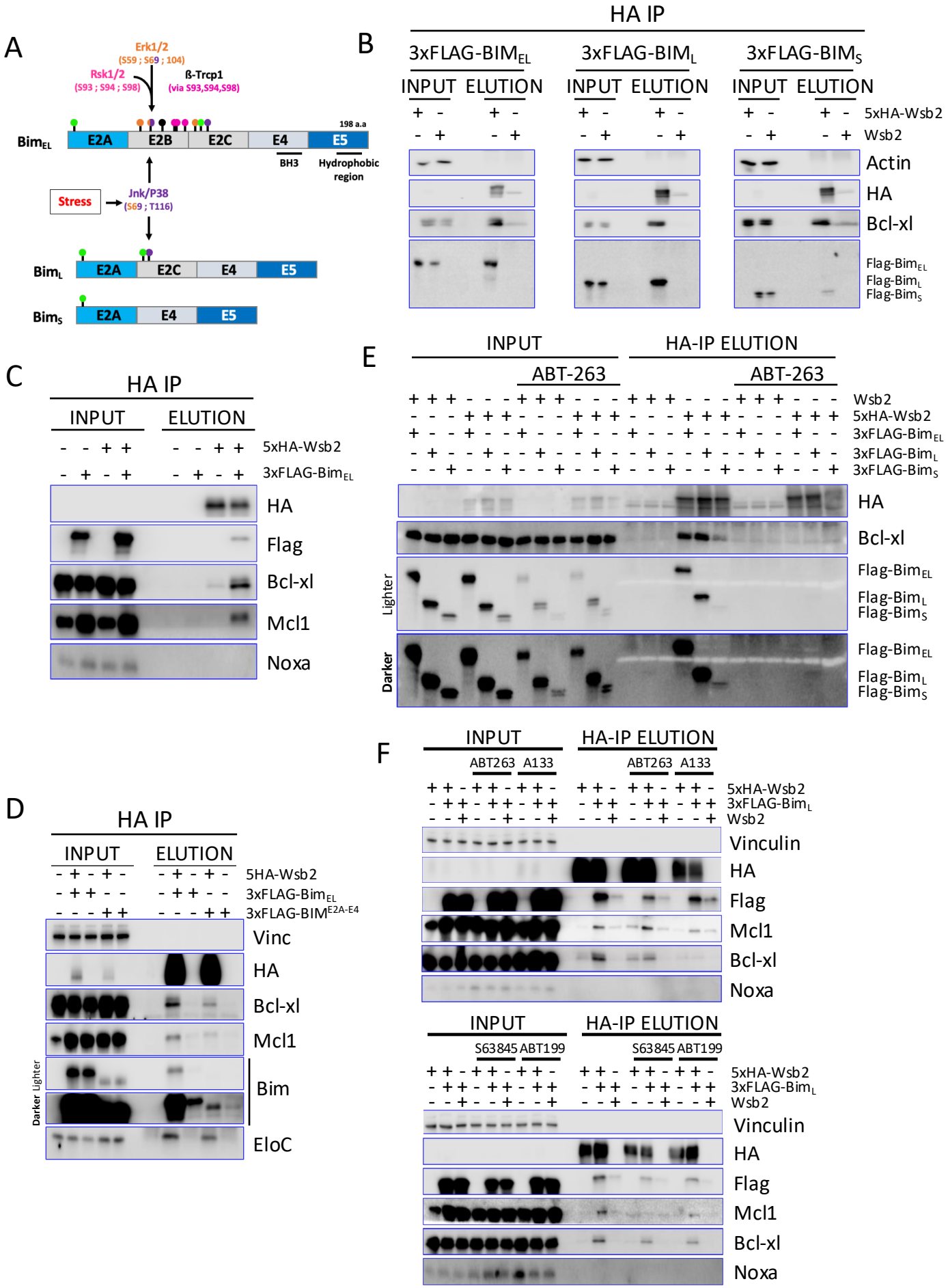
A
Erk1/2
(S59 ; S69 ; 104)
Rsk1/2
(S93 ; S94 ; S98)
ß-Trcp1
(via S93,S94,S98)
198 a.a
Bim$_{EL}$
E2A
E2B
E2C
E4
E5
BH3
Hydrophobic region
Stress
Jnk/P38
(S69 ; T116)
Bim$_L$
E2A
E2C
E4
E5
Bim$_S$
E2A
E4
E5
B
HA IP
3xFLAG-BIM$_{EL}$
3xFLAG-BIM$_L$
3xFLAG-BIM$_S$
INPUT ELUTION
5xHA-Wsb2
Wsb2
Actin
HA
Bcl-xl
Flag-Bim$_{EL}$
Flag-Bim$_L$
Flag-Bim$_S$
C
HA IP
INPUT
ELUTION
5xHA-Wsb2
3xFLAG-Bim$_{EL}$
HA
Flag
Bcl-xl
Mcl1
Noxa
E
INPUT
HA-IP ELUTION
ABT-263
ABT-263
Wsb2
5xHA-Wsb2
3xFLAG-Bim$_{EL}$
3xFLAG-Bim$_L$
3xFLAG-Bim$_S$
HA
Bcl-xl
Lighter
Darker
Flag-Bim$_{EL}$
Flag-Bim$_L$
Flag-Bim$_S$
D
HA IP
INPUT
ELUTION
5HA-Wsb2
3xFLAG-Bim$_{EL}$
3xFLAG-BIM^{E2A-E4}
Vinc
HA
Bcl-xl
Mcl1
Darker Lighter
Bim
EloC
F
INPUT
HA-IP ELUTION
ABT263 A133
ABT263 A133
5xHA-Wsb2
3xFLAG-Bim$_L$
Wsb2
Vinculin
HA
Flag
Mcl1
Bcl-xl
Noxa
INPUT
HA-IP ELUTION
S63845 ABT199
S63845 ABT199
5xHA-Wsb2
3xFLAG-Bim$_L$
Wsb2
Vinculin
HA
Flag
Mcl1
Bcl-xl
Noxa

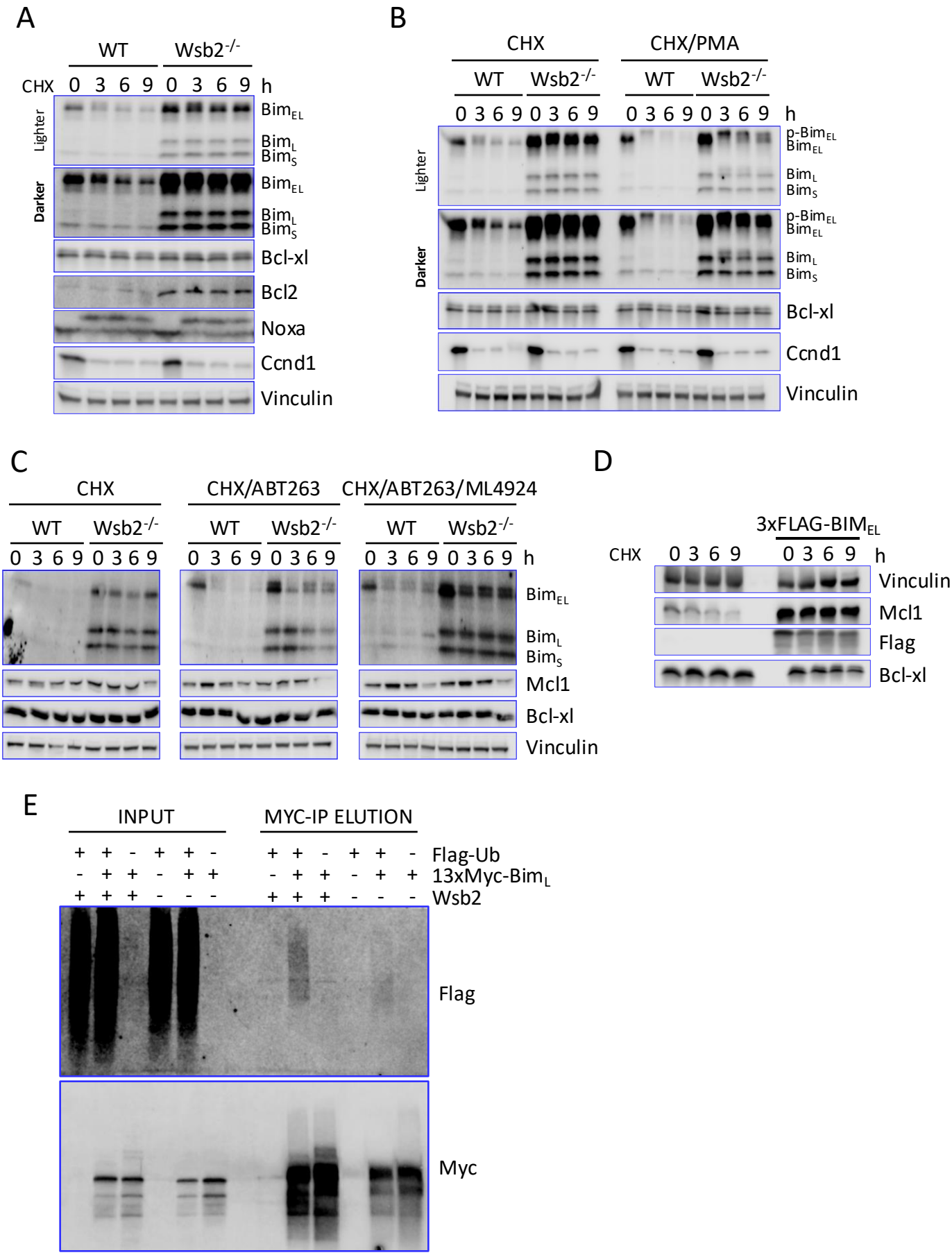
A
WT
Wsb2-/-
CHX 0 3 6 9 0 3 6 9 h
Lighter
Darker
BimEL
BimL
BimS
Bcl-xl
Bcl2
Noxa
Ccnd1
Vinculin
B
CHX
CHX/PMA
WT
Wsb2-/-
0 3 6 9 0 3 6 9 0 3 6 9 0 3 6 9 h
p-BimEL
BimEL
BimL
BimS
Bcl-xl
Ccnd1
Vinculin
C
CHX
CHX/ABT263
CHX/ABT263/ML4924
WT
Wsb2-/-
0 3 6 9 0 3 6 9 h
BimEL
BimL
BimS
Mcl1
Bcl-xl
Vinculin
D
3xFLAG-BIMEL
CHX 0 3 6 9 0 3 6 9 h
Vinculin
Mcl1
Flag
Bcl-xl
E
INPUT
MYC-IP ELUTION
+ + - + + - + + - + + -
- + + - + + - + + - + +
+ + + - - - + + + - - -
Flag-Ub
13xMyc-BimL
Wsb2
Flag
Myc

A

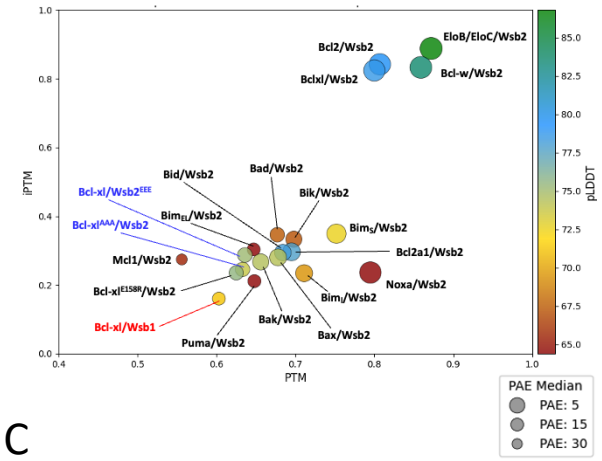
iPTM
PTM
pLDDT
Bcl2/Wsb2
EloB/EloC/Wsb2
Bclxl/Wsb2
Bcl-w/Wsb2
Bid/Wsb2
Bad/Wsb2
Bik/Wsb2
Bcl-xl/Wsb2EEE
BimEL/Wsb2
Bcl-xlAAA/Wsb2
Bim5/Wsb2
Bcl2a1/Wsb2
Mcl1/Wsb2
Noxa/Wsb2
Bcl-xlE158R/Wsb2
Bim1/Wsb2
Bcl-xl/Wsb1
Bak/Wsb2
Bax/Wsb2
Puma/Wsb2
PAE Median
PAE: 5
PAE: 15
PAE: 30

B

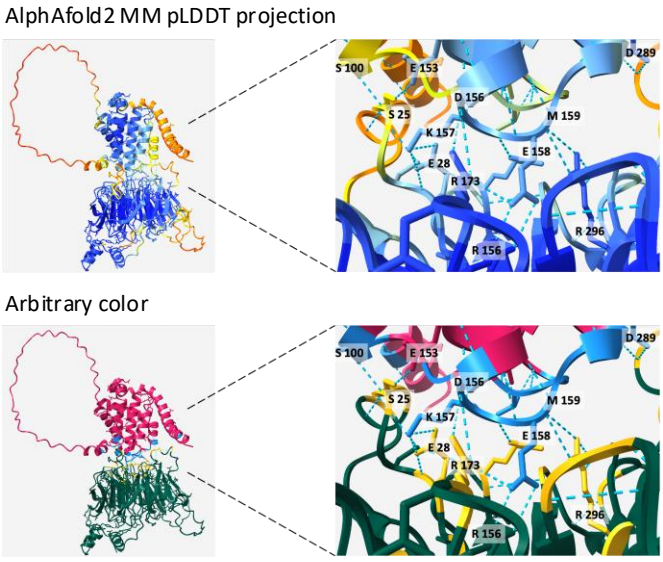
AlphAfold2 MM pLDDT projection
Arbitrary color
S 100
E 153
D 289
D 156
S 25
M 159
K 157
E 158
E 28
R 173
R 296
R 156

C

BIMEL PRMVILRLLRYIVRLVWRMH
MCL1 SRVM-IHVFSDGV-TNWGRIVTLISFGAFVAKHLKTINQESCIEPLAESITDVLV
BCL2 ATVV-EELFRDGV--NWGRIVAFFEFGGVMCVESVNREMSPLVDNIALWMTEYLN
BCLxL EQVV-NELFRDGV--NWGRIVAFFSFGGALCVESVDKEMQVLVSRIAAWMATYLN
BCLw TQVS-DELFQGGP--NWGRLVAFFVFGAALCAESVNKEMEPLVGQVQEWMVAYLE

D

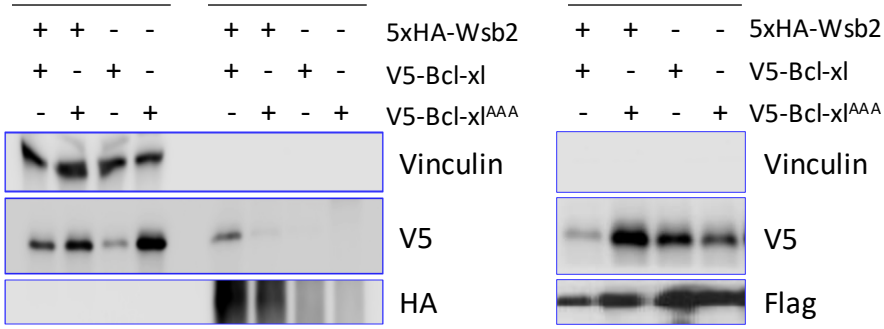
3FLAG-BimEL
INPUT
HA-IP ELUTION
3FLAG-BimEL
V5-IP ELUTION
5xHA-Wsb2
V5-Bcl-xl
V5-Bcl-xlAAA
Vinculin
V5
HA
Vinculin
V5
Flag

E

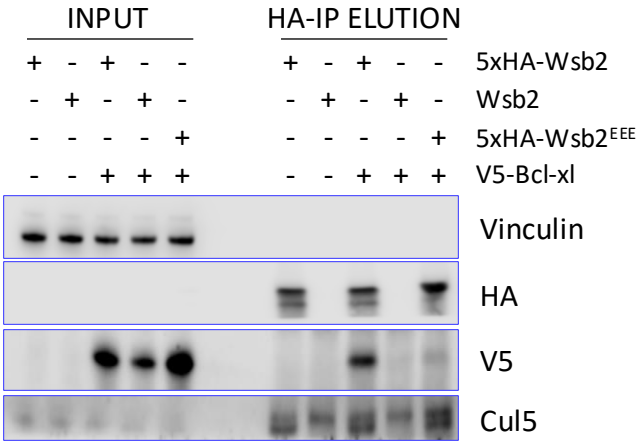
3FLAG-BimEL
INPUT
HA-IP ELUTION
5xHA-Wsb2
Wsb2
5xHA-Wsb2EEE
V5-Bcl-xl
Vinculin
HA
V5
Cul5

F

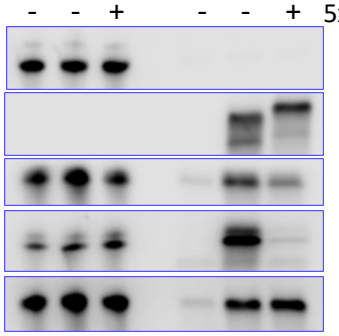
3FLAG-BimEL
INPUT
HA-IP ELUTION
5xHA-Wsb2
Wsb2
5xHA-Wsb2EEE
Vinculin
HA
Bim
Bcl-xl
Mcl1

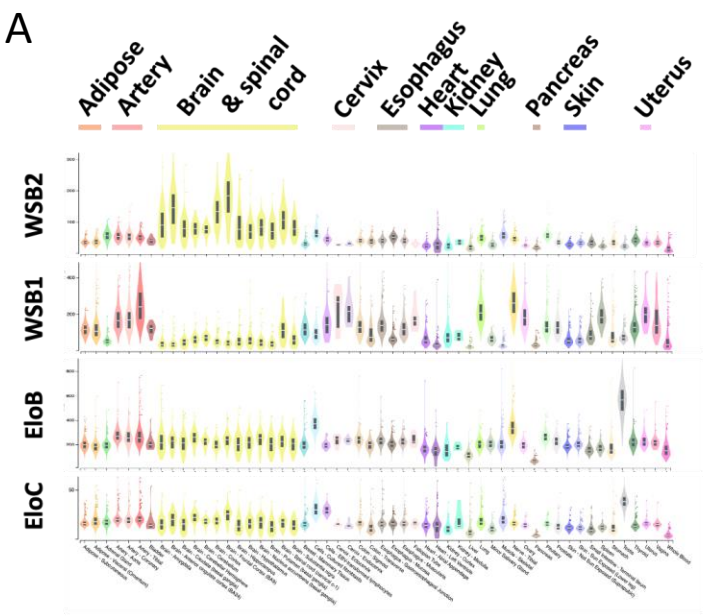
A
Adipose
Artery
Brain
& spinal cord
Cervix
Esophagus
Heart
Kidney
Lung
Pancreas
Skin
Uterus
WSB2
WSB1
EloB
EloC

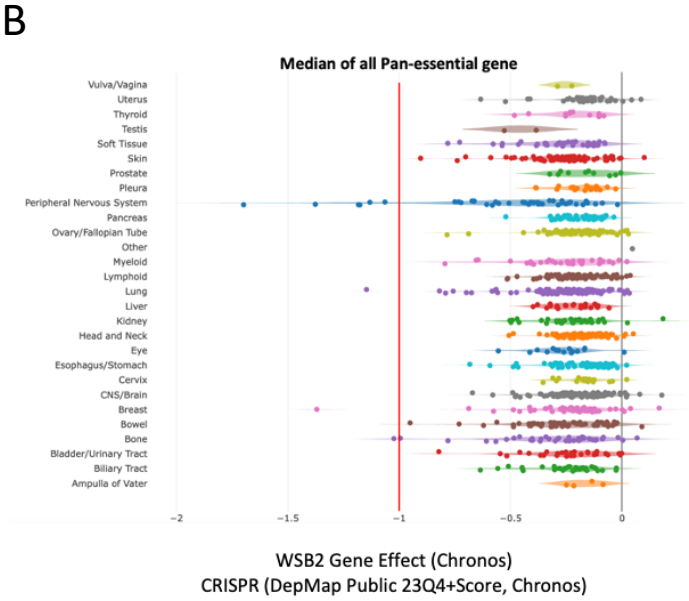
B
Median of all Pan-essential gene
Vulva/Vagina
Uterus
Thyroid
Testis
Soft Tissue
Skin
Prostate
Pleura
Peripheral Nervous System
Pancreas
Ovary/Fallopian Tube
Other
Myeloid
Lymphoid
Lung
Liver
Kidney
Head and Neck
Eye
Esophagus/Stomach
Cervix
CNS/Brain
Breast
Bowel
Bone
Bladder/Urinary Tract
Biliary Tract
Ampulla of Vater
−2
−1.5
−1
−0.5
0
WSB2 Gene Effect (Chronos)
CRISPR (DepMap Public 23Q4+Score, Chronos)

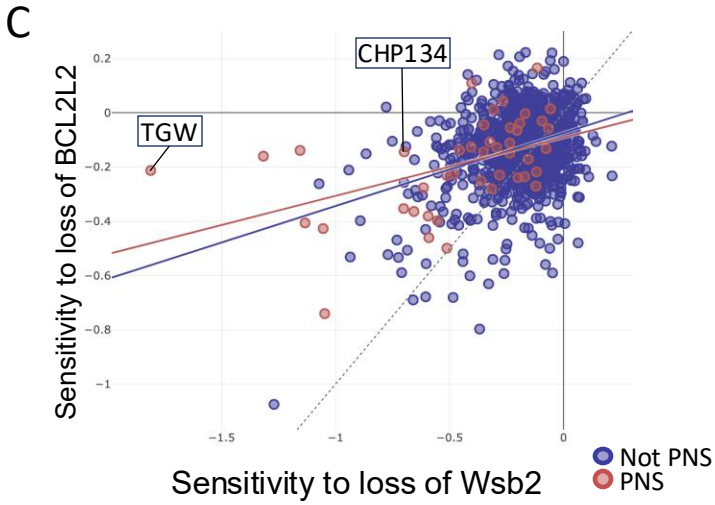
C
CHP134
TGW
Sensitivity to loss of BCL2L2
Sensitivity to loss of Wsb2
Not PNS
PNS

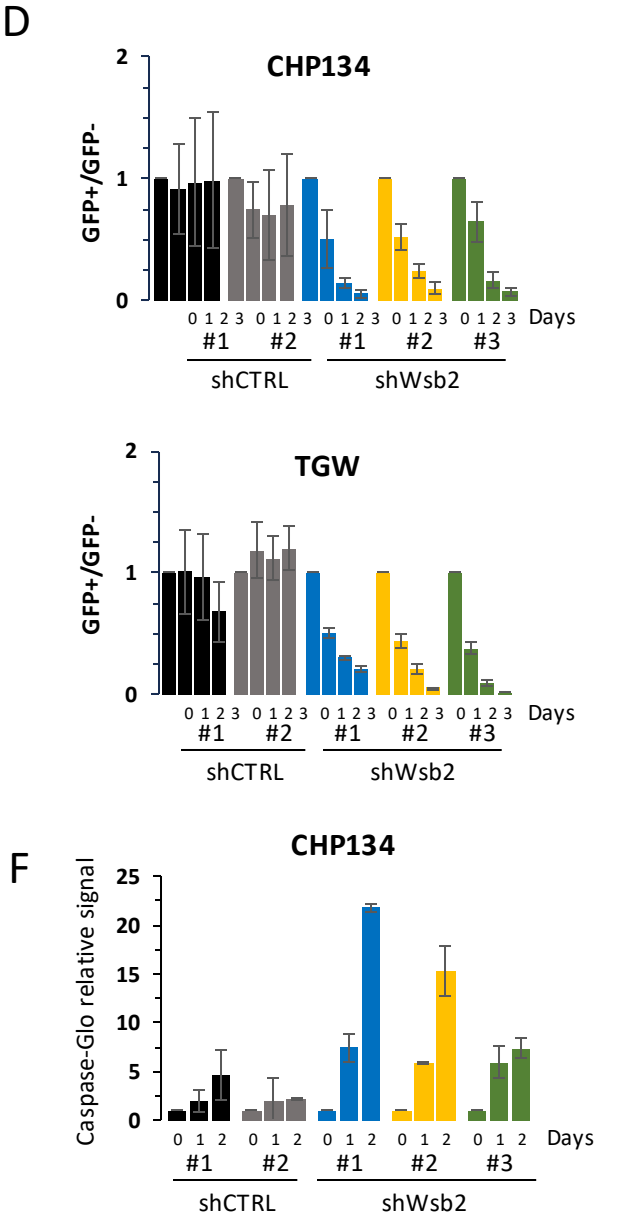
D
CHP134
GFP+/GFP-
0 1 2 3 0 1 2 3 0 1 2 3 0 1 2 3 0 1 2 3 Days
#1 #2 #1 #2 #3
shCTRL
shWsb2
TGW
F
CHP134
Caspase-Glo relative signal
0 1 2 0 1 2 0 1 2 0 1 2 0 1 2 Days
#1 #2 #1 #2 #3
shCTRL
shWsb2

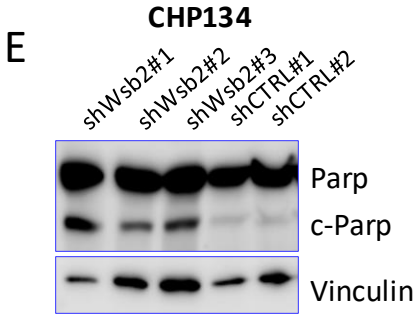
E
CHP134
shWsb2#1
shWsb2#2
shWsb2#3
shCTRL#1
shCTRL#2
Parp
c-Parp
Vinculin